

## DEVELOPMENT OF HIGH-ORDER COMPUTATIONAL TOOL TO SOLVING ACOUSTIC PROPAGATION PROBLEMS

**Saulo Ferreira Maciel, saulofmaciel@yahoo.com.br**

**Bruno Souza Carmo, bruno.carmo@usp.br**

Escola Politécnica da Universidade de São Paulo, São Paulo, Brazil

**Abstract.** *The development of a Computational Fluid Dynamic Tool based on the Finite Element Method with discontinuous Galerkin scheme is presented in this work. The aim of this study is to solve the compressible linearized Euler's equation in two dimensions on structured and non-structured meshes. This tool has been used to study sound propagation phenomena. The Riemann's problem presented on a convective flow in Euler's equation is tackled by a HLL's method and the time integration being used is the four-stage Runge-Kutta explicit method with second order of accuracy. An analytically prescribed source term was used to validate the implementation and a monopole, a dipole and a quadrupole source of sound in subsonic and supersonic flows were simulated. The computational efficiency, the convergence and the accuracy of the method were tested by comparing the simulation results against the analytical solution for the first problem and against the solutions based on Green's functions for the other ones. The convergence rate for high approximation order is asymptotic; this result is compatible with a discontinuous Galerkin formulation.*

**Keywords:** *discontinuous Galerkin, linearized Euler equation, acoustics*

### 1. INTRODUCTION

The noise generated by machines is an important problem in modern life and the community is looking for a way to study and understand it. Since Sir. James Lighthill in 1952 proposed his acoustic analogy, it has been used successfully to compute the sound propagation. At that time the target was to study jet noise. However, significant progress was made in sound propagation prediction tools, so as other noise sources beside the jet started to be investigated in the aerospace industry. Starting from the Lighthill's analogy, many others analogies were proposed. Still in the fifties, Curle (1955) presented a model of dipoles arising from solid structures and a little more than ten years later, Ffwoes Willians and Hawkings (1969) proposed that the aerodynamically-generated noise was composed by monopoles, dipoles and quadrupoles arising from pressure loading, thickness loading and turbulence respectively.

With these analogies the sound generation was uncoupled from the sound propagation. The sound propagation was easier to simulate because it can be modeled by a second order differential in terms of the pressure fluctuations, so linear governing equations can be successfully employed. On the other hand, the sound generation has not been precisely represented by linearization because the sound sources depends of complex interaction mechanisms between the physical quantities (Rienstra and Hirschberg, 2004). The stochastic noise generation and propagation approach proposed by Béchara *et al.* (1994) arise as a good alternative for the linearizations of the sound sources. However, the fast development of new numerical tools in the last years produced algorithms able to overcome many of the challenges. One of the main limitations of the first numerical tools was the excessive numerical dispersion and dissipation (Tam, 2004), so some effort has been done on that area.

High-order methods have been proved to be efficient for solving sound propagation problems and in particular the discontinuous Galerkin (DG) method has the easiness of parallelization as one of its strong features to cope with the high computational cost. The DG can be viewed as an extension of the finite volume method by using a polynomial base to represent the quantities rather than their average value or as a traditional finite element method where continuity between the elements is however not required. The elements are independent and the only communication is through a flux on their adjacent boundaries and the result of this approach is a block diagonal global mass matrix. The Riemann problem stemming from the discontinuities can be solved by an upwind method which keep the solution stable in subsonic or supersonic flows.

Trying to use these features together, we implemented a linearized compressible Euler equation (LEE) solver using the Nektar++ (www.nektar.info, 2006) library in order to simulate sound propagation using a discontinuous Galerkin scheme. We present results using the source terms defined by Bailly and Juvé (2000) and compare with reference data. The sound spreading is analyzed in the middle field (E.Mahona *et al.*, 2004), not so close from the turbulence sources neither so far where the acoustic perturbation should be measured by integrals methods.

## 2. NUMERIC FORMULATION

### 2.1 Linearized Euler equation

The starting point is to consider that the sound waves represent small perturbations around the steady mean flow. With this hypothesis, the LEE is able to capture all sound properties (Rienstra and Hirschberg, 2004). So lets consider the mean flow described by the quantities  $\mathbf{U}^t = (\rho_0, \rho_0 u, \rho_0 v, p_0)$  which represents the density, momentum in  $x$  and  $y$  directions and the pressure respectively, and the perturbations around this quantities  $(\rho', \rho_0 u', \rho_0 v', p')$ . The LEE can be stated in vectorial form around a stationary mean flow as (Bogey *et al.*, 2002)

$$\frac{\partial \mathbf{U}}{\partial t} + \frac{\partial \mathbf{E}}{\partial x} + \frac{\partial \mathbf{F}}{\partial y} + \mathbf{H} = \mathbf{S}. \quad (1)$$

The vector  $\mathbf{H}$  contains terms related to the gradients of the mean flow, which are equal to zero when the mean flow is uniform. The vector  $\mathbf{S}$  represents possible unsteady sources in the flow. There are other LEE forms but Blom (2003) shows that all of them are equivalent.

#### 2.1.1 Discontinuous Galerkin formulation

For the spatial discretization, a Discontinuous Galerkin approach is used. Its main advantages are the compactness of the method and its locality. Regardless of the order used, an element only needs information from the elements with which it has common boundaries. Considering the LEE in Eq. (1) written as a conservative differential system:

$$\frac{\partial \mathbf{U}}{\partial t} + \frac{\partial}{\partial x} F(\mathbf{U}) = \mathbf{S}, \quad (2)$$

lets develop the discretization for a scalar unknown  $u$  and the results can be extended to vectorial unknowns. First consider that the solution of Eq. (2) can be represented by a sum of  $P + 1$  analytical functions named trial functions

$$u(x, t) \approx u^\tau(x, y) = \sum_{i=0}^P \hat{u}_i(t) \phi_i(x), \quad (3)$$

which should satisfy the initial and boundary conditions. Let's split the domain  $\Omega$  in  $N_{el}$  non-overlapping subdomains

$$\Omega = \bigcup_{e=1}^{N_{el}} \Omega^e, \quad \bigcap_{e=1}^{N_{el}} \Omega^e = \partial \Omega^e. \quad (4)$$

To construct the variational form (or weak form), lets replace the approximate solution Eq. (3) in Eq. (2), multiply by an analytical function  $v_j(x)$ , named test function, integrate over the element  $\Omega^e$  and apply the divergence theorem over the second member to obtain

$$\frac{\partial}{\partial t} \int_{\Omega^e} v_j u^\tau d\Omega^e + \int_{\partial \Omega^e} v_j^\tau \hat{f}(u_+, u_-) \cdot n d\partial \Omega^e - \int_{\Omega^e} u^\tau \frac{\partial v_j}{\partial x} d\Omega^e = \int_{\Omega^e} v_j s d\Omega^e. \quad (5)$$

The term  $\hat{f}(u_+, u_-)$  is known as numerical flux. Considering that the trial and the test functions are the same, the discontinuous Galerkin is defined by: Find  $v, \phi \in L^2$  which satisfies Eq. (5) for all  $\Omega^e \in \Omega$ , where  $L^2$  is the Lebesgue space, or simply square-integrable space functions.

### 2.2 Numerical flux

The numerical flux is solved as a Riemann problem because we assumed the existence of a discontinuity over  $\Omega^e$  and  $\Omega^{e+1}$  boundaries. The discontinuity is only local because the numerical flux is explicitly calculated and it is responsible to keep the global solution continuous. There are a number of upwind methods to calculate an approximation to the numerical flux that can be cited, for example Lax-Friedrichs (Chu, 1978), Roe (Roe, 1981), HLL and HLLC (Harten *et al.*, 1983). The simplest one is the Lax-Friedrichs but it makes the algorithm unstable so we used the HLL method. Knowing that the eigenvalues of the Jacobian matrix from Euler's equation are  $(u + c_0, u, u - c_0)$ , where  $c$  is the speed of sound, the numerical flux calculated by the HLL method reads

$$\hat{f}(u_+, u_-) = \begin{cases} f(u_-) & \text{if } S_L \leq 0 \\ \frac{S_R f(u_-) - S_L f(u_+) + S_R S_L (u_+ - u_-)}{S_R - S_L} & \text{if } S_L \leq 0 \leq S_R \\ f(u_+) & \text{if } S_R \leq 0 \end{cases} \quad (6)$$

where  $S_L = \max(u \pm c_0)$  e  $S_R = \min(u \pm c_0)$ .

### 2.3 Time integration

To choose amongst the many time integration methods available, two points merit attention in a DG implementing. First the discontinuous character of the method is local and this often leads to standard explicit structures, so explicit methods are preferred for discontinuous finite elements formulations although there are no impediments to use implicit methods. Second, since the explicit methods are prone the numerical instability, a stability analysis is required for proper use of these methods and therefore stability criteria were established for temporal integration problems most commonly used for flow fluids and heat transfer (Li, 2006). In this work, the system of ordinary differential equations was solved explicitly by means of a 4-steps Runge-Kutta method, and the time-step was calculate so as to make the Courant-Friedrich-Lewy (CFL) number equal to 1.

## 3. NUMERICAL RESULTS

### 3.1 Validation

To validate the implementation accuracy we used a well known validation method which was employed in a similar way by Karniadakis and Sherwin (2005). In this method the vectorial function

$$\mathbf{U} = \begin{pmatrix} 14 \\ \sin x \\ \cos y \\ 10 \end{pmatrix} \beta \sin(t) e^{-\alpha(x^2+y^2)}, \quad (7)$$

with  $\alpha = 10^{-2}$  and  $\beta = 10^{-3}$  is replaced on the left hand side (LHS) of Eq. (1) deriving the right hand side (RHS). Then we set the uniform mean flow with the values of Tab. 1 for Mach = 0.5 and ran the software replacing the source term  $\mathbf{S}$  in Eq. (1) by the RHS from the analytical function. The simulation time was  $t=10.5$  and polynomial orders  $P = 1 - 19$  were tested. Three meshes wre employed: a structured mesh with 81 squares and two unstructured meshes, the first with 110 triangles and the second with 27 triangles and 83 quadrilaterals. All of them covered the domain  $-100 \leq x, y, \leq 100$ . To compare the results, the  $L^2$  norm from the difference between the numerical solution and the analytic function was calculated.

Table 1. Uniform mean flow values for primitive variables

Variable	Mach 0.0	Mach 0.5	Mach 2.0
$\rho_0$	1.4	1.4	1.4
$u_0$	0.0	0.5	2.0
$v_0$	0.0	0.0	0.0
$p_0$	1.0	1.0	1.0

We expected an exponential convergence but we found an asymptotic behavior of the convergence instead. For the structured mesh, Fig. 1(a), and for the mixed unstructured mesh, Fig. 1(c), we found a small oscillation and for  $P = 10$  the error almost stabilizes, suggesting that the calculations reached machine error levels. This hypothesis is confirmed by evaluating the magnitude difference of the simulations. The the simplest case,  $P = 1$ , involved 324 integration points, or degrees of freedom, with 210 time steps, while the more complex,  $P = 19$ , had 32,400 integration points and 2625 time steps and flops ranged from  $10^{10}$  to  $10^{14}$  for the simplest to the most complex cases respectively. The triangular mesh, Fig. 1(b) shows smaller errors. This result was unexpected but not surprising. The Nektar++ uses the variable expansion polynomial base, see (Karniadakis and Sherwin, 2005) and the triangular regions are the natural space of this base.

Figure 2 shows a convergence study for the mesh and polynomial refinement. Babuska and Suri (1994) states that the  $hp$  technique seeks to group the results of exponential convergence ( $p$  refinement) and arithmetic convergence ( $h$  refinement). So let's analyze the  $hp$  convergence of the previous problem. Fig. 2(a) shows the  $hp$  convergence obtained by five successive divisions of a four square meshes with polynomial orders varying from  $P = 1$  to  $P = 6$  and with characteristic mesh lenghts following the sequence  $h = (1, 0.5, 0.25, 0.125, 0.0625)$ . The isolated behavior of  $h$  and  $p$  convergence is analysed in Fig. 2(b). In this case  $P = 3$  was fixed and the four square elements mesh was refined following decreasing sequence  $h = (1, 0.5, 0.25, 0.125, 0.0625)$ . After that, the 16 square elements mesh ( $h=0.5$ ) was fixed and the polynomial orders  $P = (2, 3, 4, 7, 10, 12, 20)$  were tested. As expected, the  $h$  convergence is arithmetic while the  $p$  convergence is exponential.

If DG methods, the convergence of the error is exponential and the computational effort follows the same tendency. With increasing polynomial order, better convergence results were obtained but this requires greater computational effort as showed in Fig. 1(d) where the trend line is exponential with a good correlation coefficient. This is the DG disadvantage but this feature may be offset by its parallelism advantages, as showed by Crivellini and Bassi (2003) and Wilcox *et al.* (2010).

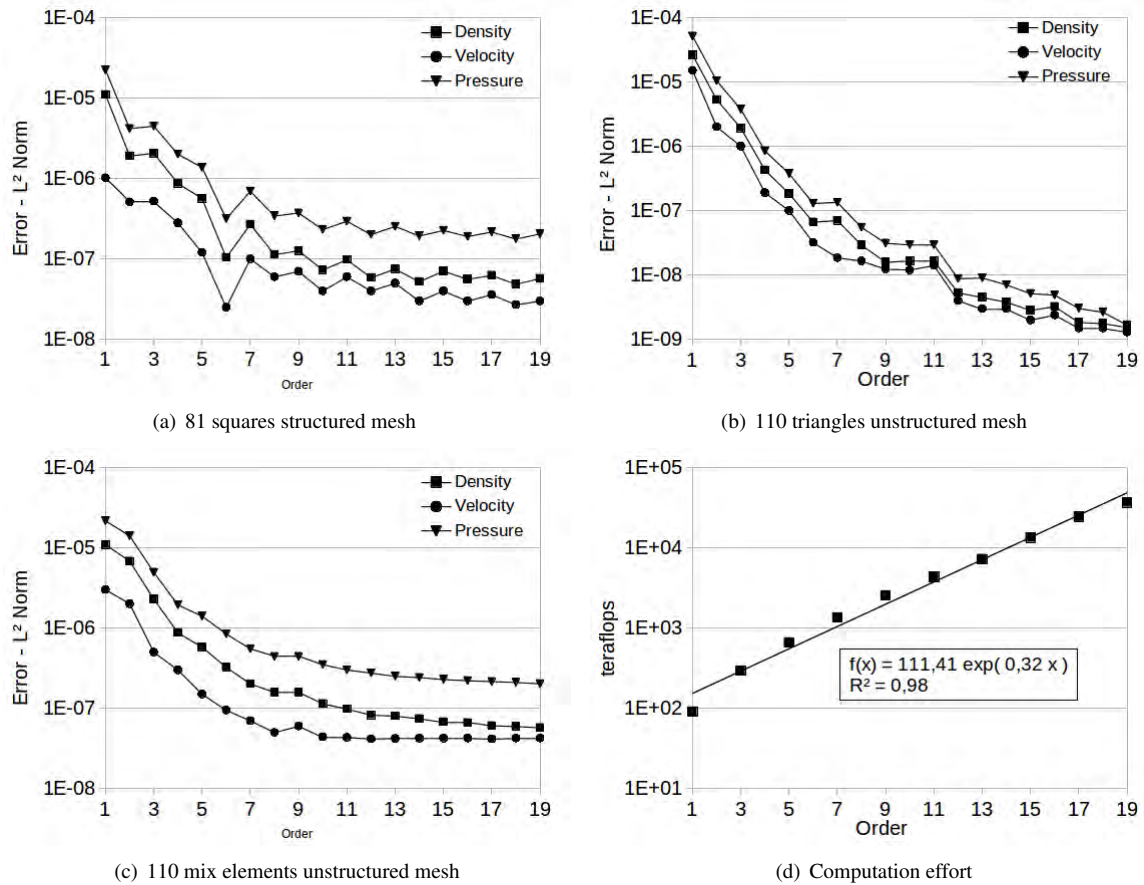
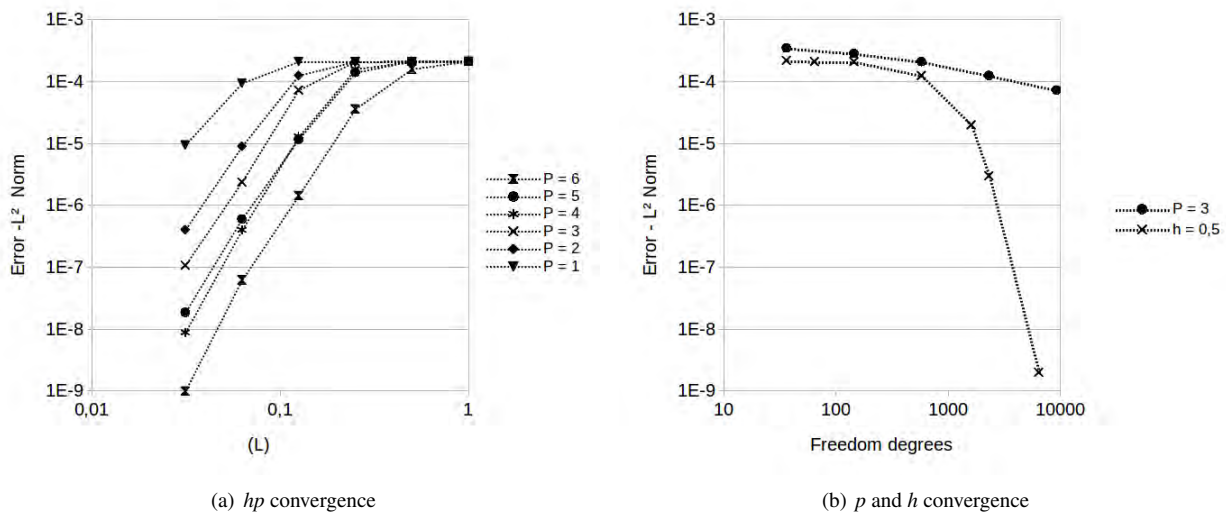
Figure 1.  $L^2$  norm error convergence.

Figure 2. Error convergence for different characteristic length mesh.

### 3.2 Monopolar source

This subsection presents the propagation of a monopole source of sound in a subsonic and supersonic mean flow as presented by Bailly and Juvé (2000). This problem is mathematically modeled by inserting the source  $\mathbf{S} = f(x, y) \sin \omega t \times [\beta, 0, 0, \beta/\gamma]^T$  in the LEE, Eq. (1) where  $f(x, y) = e^{-\alpha[(x-x_s)^2+(y-y_s)^2]}$ .  $\alpha, \beta$  are constants,  $\omega$  is the angular frequency and  $(x_s, y_s)$  are the source coordinates. All these parameters have a different value for the subsonic and supersonic cases presented below. The analytic solution for the pressure field is based on the convolution product  $p(x, y, t) =$

$f(x, y) * dG/dt(x, y, t)$  where  $G$  is the Green function given by

$$G(x, y, t) = \frac{i}{4c_0} \frac{1}{\sqrt{1-M^2}} H_0 \left[ k \frac{\sqrt{x^2 + (1-M^2)y^2}}{1-M^2} \right] \exp \left( -i \frac{M}{1-M^2} kx - i\omega t \right), \quad (8)$$

for the subsonic flow and

$$G(x, y, t) = \frac{1}{2c_0} \frac{1}{\sqrt{M^2-1}} J_0 \left[ k \frac{\sqrt{x^2 + (M^2-1)y^2}}{M^2-1} \right] \exp \left( -i \frac{M}{M^2-1} kx - i\omega t \right) \quad (9)$$

supersonic flow which were deduced by Bailly and Juvé (2000) where  $M$  is the Mach number,  $H_0$  and  $J_0$  are the Hankel and Bessel zero order first kind functions respectively. Both subsonic and supersonic were simulated in a  $9 \times 9$  squares structured mesh with dimension  $-100 \leq x, y \leq 100$ .

### 3.2.1 Subsonic flow

The monopole propagation in subsonic flow (Mach=0.5) is achieved by using the source term  $\mathbf{S}$  in Eq. 1 with the parameters  $\alpha = \ln(2)/2$ ,  $\beta = \rho_0/100$ ,  $\omega = \pi/15$  and  $(x_s, y_s) = (-30, 0)$ . The mean flow has the values of the Tab. 1. The pressure disturbances for  $t = 40, 70, 100, 130$  are showed in Fig. 3. Fig. 4 shows the pressure profile over the line  $y = 0$ ,  $t = 150$  and  $P = 19$ ; the numerical data is indistinguishable from the analytical solution. Recalling that the wave speed is given by  $v = 2\pi\lambda/\omega$ , it is possible to see in the same figure the upstream and downstream waves propagating with speed  $v_0$  and  $3v_0$  matching with  $(1 \pm M)$  and these results say that the software solve such problems efficiently.

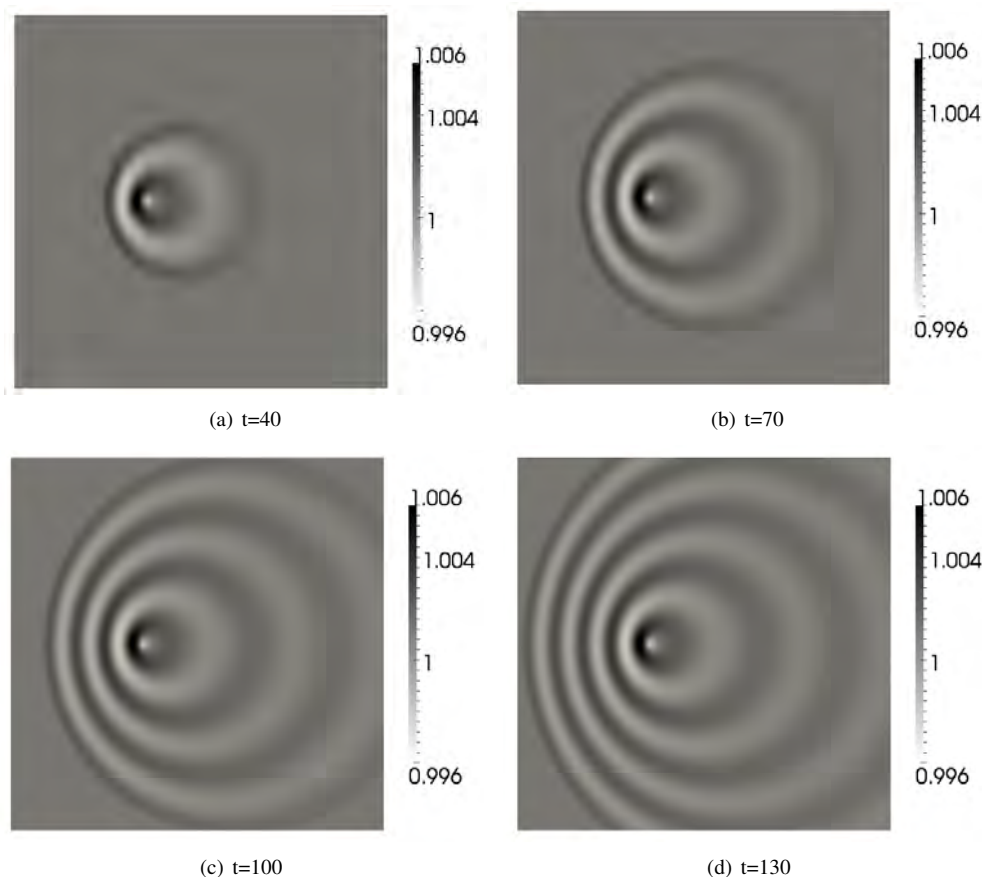


Figure 3. Pressure surface in subsonic flow - Mach=0.5 and P=19

### 3.2.2 Supersonic flow

The monopole propagation in supersonic flow (Mach=2.0) is similar to the previous problem with parameters  $\alpha = -\ln(2)/5$ ,  $\beta = \rho_0/25$ ,  $\omega = \pi/5$ ,  $(x_s, y_s) = (-50, 0)$  and uniform mean flow values from Tab. 1. The pressure disturbances at  $t = 50, 100, 150, 250$  and  $P = 19$  is showed in Fig. 5 where the Mach cone defined in cylindrical coordinates by  $M \sin \theta = 1$  has  $\theta \approx 29.4^\circ$  which is in agreement with Mach = 2.0. Besides this, the overlapping waves propagating downstream with speeds  $M \pm 1$  can be observed. Figure 6 shows the pressure profile for  $y = 0$ ,  $t = 250$  and

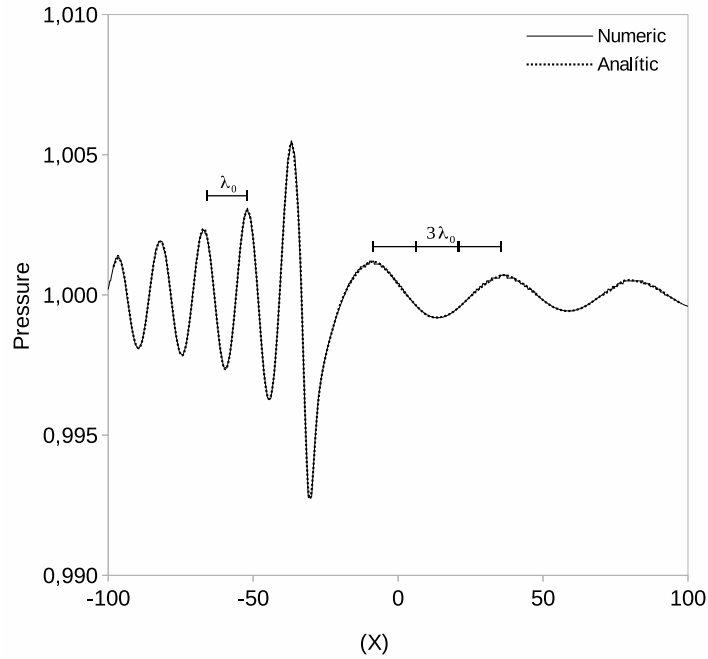


Figure 4. Subsonic monopole pressure profile -  $y=0$ , Mach=0.5,  $P=19$  and  $t=150$

$P = 19$ . Small differences appear between the analytical and numerical solution but in general the problem was well resolved. We suppose that better results can be achieved by introducing a selective damping schema as proposed in Tam *et al.* (1993).

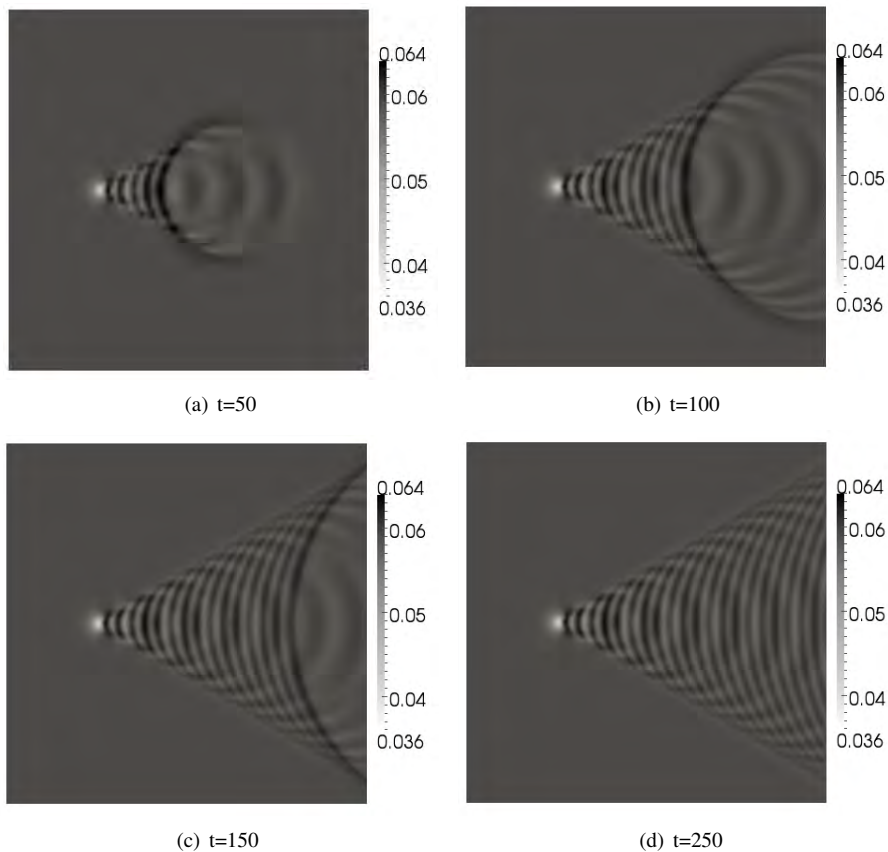
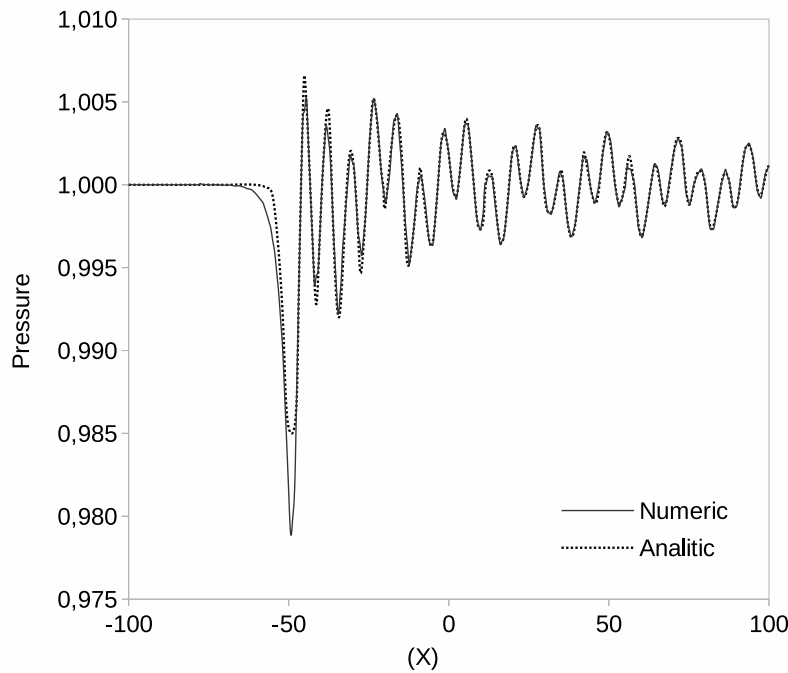


Figure 5. Pressure surface in supersonic flow - Mach=2.0 and  $P=19$

Figure 6. Subsonic monopole pressure profile -  $y=0$ , Mach=2.0,  $P=19$  and  $t=250$ 

### 3.3 Multipolar source

Starting from the mass conservation and momentum conservation equations with source terms it is possible to write the perturbed wave equation (Rienstra and Hirschberg, 2004)

$$\frac{\partial^2 p'}{\partial t^2} - c_0^2 \frac{\partial^2 p'}{\partial x_j^2} = \mathbf{S}. \quad (10)$$

If  $\mathbf{S} = \partial F_i / \partial x_i$  and

$$\int_V \frac{\partial F_i}{\partial x_i} = \int_S F_i dS = 0, \quad \int_V F_i dx \neq 0 \quad (11)$$

the source  $\mathbf{S}$  represents a dipole and the analytical solution is given by the convolution product  $p' = -F_i * \partial G / \partial x$  where  $G$  is the Green function

$$G(x, y, t) = \frac{i}{4c_0} H_0^{(1)} \left[ \frac{\omega}{c_0 \sqrt{x^2 + y^2}} \right] e^{-i\omega t}. \quad (12)$$

On the other hand, if  $\mathbf{S} = \partial^2 T_{ij} / \partial x_i \partial x_j$  and

$$\int_V \frac{\partial^2 T_{ij}}{\partial x_i \partial x_j} = 0, \quad \int_V \frac{\partial T_{ij}}{\partial x_j} = 0, \quad (13)$$

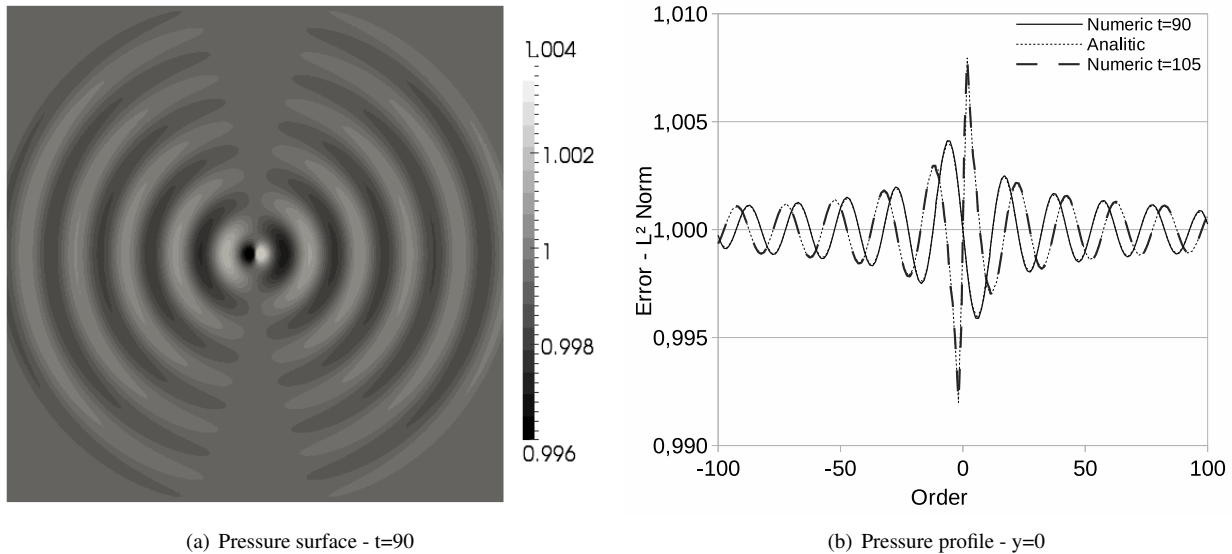
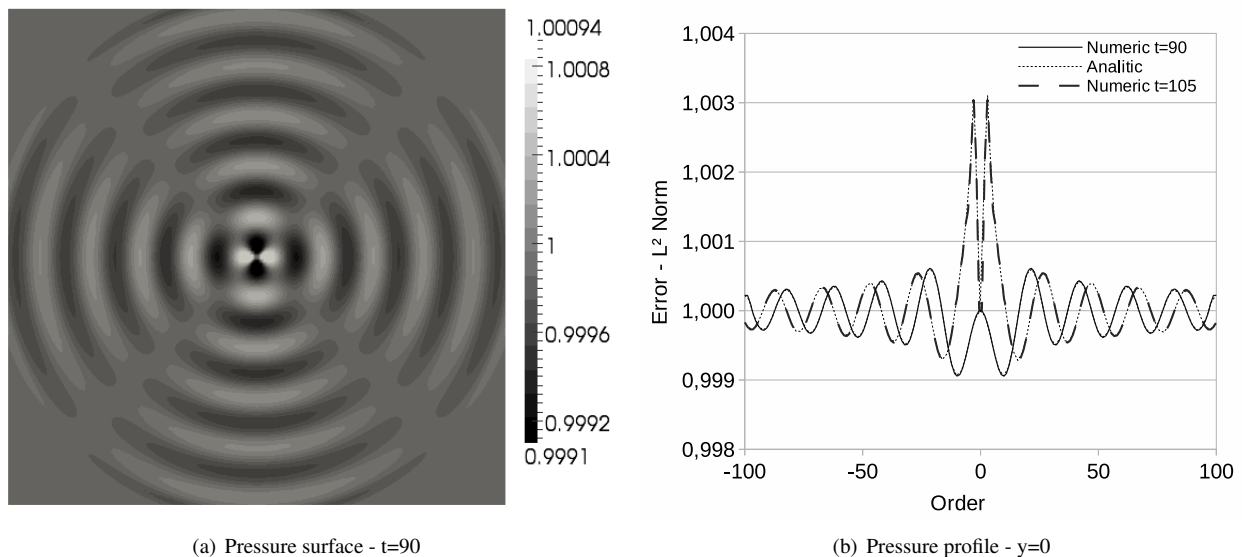
then  $\mathbf{S}$  represents a quadrupole where the solution is the sum of the convolution product  $p' = \partial F_{11} / \partial x * \partial G / \partial x + \partial F_{22} / \partial y * \partial G / \partial y$  where  $G$  is the Green function given by Eq. (12). Both dipole and quadrupole were simulated in a  $9 \times 9$  squares structured mesh with dimension  $-100 \leq x, y \leq 100$ .

#### 3.3.1 Dipole

The dipole distribution is located in the origin and is defined by

$$f_j(\mathbf{x}, t) = -\frac{5}{\pi} \epsilon \cos\left(\frac{\pi x}{5}\right) e^{-\alpha(x^2 + y^2)} \sin(\omega t) \delta_{1j}, \quad \mathbf{S} = (0, \beta, 0, 0)^T \sin(\pi x / 5) \sin(\omega t) e^{-\alpha(x^2 + y^2)} \quad (14)$$

where  $\omega = \frac{\pi}{10}$ ,  $\beta = 0.01$  and  $\alpha = \ln(2)/2$  and the mean flow with Mach=0.0 values are in Tab. 1. Figure 7(a) shows the pressure surface for  $t = 90$  and Fig. 7(b) shows the pressure profile for  $t = 90$  and  $t = 105$  over the line  $y = 0$ , in which the numerical data matches exactly the analytical solution.

Figure 7. Dipole distribution -  $P=19$ Figure 8. Quadrupole distribution -  $P=19$ 

### 3.3.2 Quadrupole

The quadrupole distribution is located at the origin and is defined by

$$T_{ij} = \begin{bmatrix} -\cos[(\pi/5)x]e^{-\alpha(x^2+y^2)} & 0 \\ 0 & \cos[(\pi/5)y]e^{-\alpha(x^2+y^2)} \end{bmatrix} \beta \frac{5}{\pi} \sin(\omega t) \quad (15)$$

where  $\omega = \frac{\pi}{10}$ ,  $\beta = 0.01$  and  $\alpha = \ln(2)/2$  and the mean flow with Mach=0.0 values are in Tab. 1. Figure 8(a) shows the pressure surface and Fig. 8(b) shows the pressure profile for  $t = 90$  and  $t = 105$  over the line  $y = 0$ . Once again, the simulation data matches the analytical solution.

## 4. CONCLUSIONS

The DG method was proven to be an efficient tool for sound propagation simulation. The stability and accuracy were tested and the results are in excellent agreement with previously published data. Particularly, for Computational Aeroacoustics (CAA) problems it can be an interesting tool because high-order approximations are able to capture a large variety of wavelengths. The monopole, dipole and quadrupole sources studied in this work can represent some of the CAA problems. In addition, the multipolar nature of the source is preserved by the numerical scheme, a crucial point for aerodynamic noise predictions.

## 5. REFERENCES

- Babuska, I. and Suri, M., 1994. “The  $p$  and  $hp$  versions of the finite element method, basic principles and properties”. *SIAM Review*, Vol. 36, No. 4, pp. 578–632.
- Bailly, C. and Juvé, D., 2000. “Numerical solution of acoustic propagation problem using linearized Euler equations”. *AIAA Journal*, Vol. 38.
- Béchara, W., Bailly, C., Candel, S.M. and Lafon, P., 1994. “Stochastic approach to noise modeling for free turbulent flows”. *AIAA Journal*, Vol. 32, pp. 455–463.
- Blom, C., 2003. *Discontinuous Galerkin method on tetrahedral elements for aeroacoustics*. Ph.D. thesis, University of Twente, Enschede, Netherlands.
- Bogey, C., Bailly, C. and Juvé, D., 2002. “Computation of flow noise using source terms in linearized Euler’s equations”. *Aiaa Journal*, Vol. 40, pp. 235–243.
- Chu, C.K., 1978. *Numerical Methods in Fluid Mechanics, Advances in Applied Mechanics*. Academic Press.
- Crivellini, A. and Bassi, F., 2003. “A three-dimensional parallel discontinuous Galerkin solver for acoustic propagation studies”. *International Journal of Aeroacoustics*, Vol. 2, pp. 157–173.
- Curle, N., 1955. “The influence of solid boundaries upon aerodynamic sound”. *Proceedings of the Royal Society of London. Series A. Mathematical and Physical Sciences*, Vol. 231, No. 1187, pp. 505–514.
- E.Mahona, Redonnet, S., Terracol, M. and Guéanff, R., 2004. “Numerical simulation of aeroacoustics noise”. *ECCO-MAS*, Vol. 28.
- Ffwoes Willians, J.E. and Hawkings, D.L., 1969. “Sound generation by turbulence and surfaces in arbitrary motion”. *Royal Society of London Philosophical Transactions Series A*, Vol. 264, pp. 321–342.
- Harten, A., Lax, P.D. and van Leer, B., 1983. “On upstream differencing and Godunov-type schemes for hyperbolic conservation laws”. *SIAM Review*, Vol. 1, No. 25, pp. 35–61.
- Karniadakis, G.E. and Sherwin, S.J., 2005. *Spectral/hp Element Methods for Computational Fluid Dynamics*. Oxford University Press.
- Li, B.Q., 2006. *Discontinuous finite elements in fluid dynamics and heat transfer*. Springer, Germany.
- Rienstra, S. and Hirschberg, A., 2004. *An introduction to aeroacoustics*. Eindhoven University of Technology.
- Roe, P.L., 1981. “Approximate Riemann solvers, parameter vectors and difference schemes”. *Journal of Computational Physics*, Vol. 43, pp. 357–372.
- Tam, C.K.W., 2004. “Computational aeroacoustics: An overview of computational challenges and applications”. *International Journal of Computational Fluid Dynamics*, Vol. 8, pp. 547–567.
- Tam, C., Webb, J. and Dong, Z., 1993. “A study of the short wave components in computational acoustics”. *Journal of Computational Acoustics*, Vol. 1, pp. 1–30.
- Wilcox, L.C., Stadler, G., Burstedde, C. and Ghattas, O., 2010. “A high-order discontinuous Galerkin method for wave propagation through coupled elastic-acoustic media”. *Journal of Computational Physics*, Vol. 229, No. 24, pp. 9373–9396.
- www.nektar.info, 2006.

## 6. RESPONSIBILITY NOTICE

The following text, properly adapted to the number of authors, must be included in the last section of the paper:  
The author(s) is (are) the only responsible for the printed material included in this paper.